PCCP

ROYAL SOCIETY OF CHEMISTRY

PAPER

View Article Online
View Journal | View Issue

Cite this: *Phys. Chem. Chem. Phys.*, 2024, **26**, 12188

Theoretical insight into the rearrangement of sulfur atoms on the Ni- and Cu-doped MoS_2 S-edge induced by hydrogen adsorption under HDS reaction conditions†

Alba B. Vidal, *[a] Oscar Hurtado-Aular,[b] José Luis Peña-Mena,[a] Rafael Añez[a] and Aníbal Sierraalta [a]

Received 29th January 2024,
Accepted 25th March 2024

DOI: 10.1039/d4cp00418c

rsc.li/pccp

Density functional theory (DFT) calculations and an atomistic thermodynamic approach were used to study the geometric rearrangement of sulfur atoms on the Ni- and Cu-doped MoS_2 S-edge upon hydrogen adsorption. Under HDS conditions, thermodynamically stable hydrogenated structures were identified as SH groups on the undoped S-edge with 100% sulfur coverage, on the Ni-doped S-edge with 50% sulfur coverage and on the Cu-doped S-edge with 25% sulfur coverage. It was found that the rearrangement of the S atoms is essential to reach the most stable state at the edge for the undoped and Ni-doped S-edge. Hydrogen adsorption on the Ni-doped S-edge leads to the greatest amount of S rearrangement ($\Delta E_{Rearrang}$ = 0.93 eV/H_2). Our results suggest that under the reaction conditions, the H_2 dissociative adsorption process is strongly coupled to the rearrangement of the sulfur atoms. By examining the differential hydrogen adsorption energy on the most stable edge structures, we found a plausible explanation for the trend in the hydrogenation activity of the doped edges. Our results suggest that Ni enhances the hydrogenation activity of the S-edge by decreasing the S–H bond strength, while Cu poisons it by increasing the S–H bond strength.

1. Introduction

Molybdenum disulfide (MoS_2) based catalysts are commonly used in oil refineries for hydrotreating, a process that converts crude oil into clean transportation fuels.[1,2] Promoting MoS_2 with Co or Ni increases the hydrotreating activity by more than one order of magnitude, and the selectivity for the hydrodesulfurization (HDS), hydrodenitrogenation (HDN), and hydrogenation reactions is significantly modified.[3–5] The enhanced activity is attributed to the formation of the so-called "Co–Mo–S" phase.[6] The Co–Mo–S phase model, now widely accepted and adapted to Ni promotion (Ni–Mo–S phase), proposes that the Co or Ni atoms are located at the edges of the MoS_2 slabs.[7] In this context, Kibsgaard *et al.*[5] performed a comparative analysis using scanning tunneling microscopy (STM) to study the atomic-scale structure and morphology of MoS_2 nanoparticles doped with first-row transition metals (Fe, Co, Ni, and Cu). Their results showed that the addition of all four dopant metals leads to the formation of Co–Mo–S type structures, which take the shape of hexagonally truncated triangular MoS_2 nanoparticles. The dopants were found to be preferentially located on the S-edge.

Recent experimental studies have investigated the intrinsic catalytic activity of MoS_2 catalysts doped with first-row transition metals in HDS and hydrogenation reactions. These studies have shown that Ni doping enhances the catalytic activity compared to the MoS_2 reference, while Cu doping has a negative effect, reducing the catalytic activity.[5,8] The active sites on the doped and undoped MoS_2 catalysts may involve coordinatively unsaturated sites (CUSs), sulfhydryl (SH) groups, and brim sites. CUSs are vacancies of S^{2-} anions located at the edge or corner of the nanoparticles.[9] The SH groups are formed by hydrogen dissociative adsorption on the outermost edge S atoms and behave as Brønsted acid sites.[10,11] The brim sites, which can be seen in STM images as a bright brim adjacent to the MoS_2 nanoparticle edge, exhibit metallic characteristics because of the presence of one-dimensional electronic edge states.[12,13] There is a broad consensus in the literature that the HDS activity of the MoS_2-based catalyst proceeds through two parallel pathways: the direct desulfurization (DDS) pathway and the hydrogenation (HYD) pathway.[14–17] In the DDS pathway, the sulfur atom is directly removed from the molecule upon

[a] *Laboratorio de Química Física y Catálisis Computacional, Centro de Química "Dr Gabriel Chuchani", Instituto Venezolano de Investigaciones Científicas (IVIC), Apartado 21827, Caracas, Venezuela. E-mail: abvidals@gmail.com*
[b] *IFISUR, Universidad Nacional del Sur (UNS-CONICET), Av. Alem 1253, 8000, Bahía Blanca, Argentina*

† Electronic supplementary information (ESI) available. See DOI: https://doi.org/10.1039/d4cp00418c

hydrogenolysis of the C–S bond, whereas the HYD pathway involves several hydrogenation steps before sulfur extrusion occurs. For sterically hindered alkyl-substituted compounds such as 4,6-dimethyldibenzothiophene (DMDBT), the DDS pathway is often suppressed and the HYD pathway becomes the dominant pathway because it is less sensitive to steric effects. As a result, the HYD pathway becomes increasingly important as crude oils become heavier and contain more refractory compounds.[18] Both reaction pathways require the activation of H_2. It is proposed that the S–H groups, which are formed by the dissociation of H_2 at the edges, drive the hydrogenation steps that precede the sulfur extrusion process.[19,20]

Determining the state of adsorbed hydrogen on MoS_2-based catalysts is fundamental to understand the overall catalytic process of the HDS reaction. Two types of H_2 dissociation mechanisms have been proposed: heterolytic dissociation, which produces a molybdenum hydride species and an SH group, and homolytic dissociation, which produces two SH groups. Therefore, several theoretical studies have focused on the activation of H_2 by the MoS_2 edges.[21–26] Some of these studies have reported that H-adsorption induces rearrangement of the edge sulfur atoms. Specifically, the terminal S_2 dimers split upon H adsorption, resulting in a significant shift of the S atoms.[21,25,26] Tsai *et al.*[27] pointed out that adsorbates often induce significant reorganization of the S atoms at the edge. This generally involves repulsive interactions between neighboring S atoms, as well as the breaking of an S–S bond if the adsorbate is bound to an S_2 dimer. Salazar *et al.*[28] combined STM experiments and density functional theory (DFT) calculations to investigate the adsorption of thiophene on S-vacancies at the Mo-edge of MoS_2 nanoparticles. The study found that thiophene adsorbs directly on open S-vacancy sites at the corners between the edges. However, adsorption on S-vacancy sites located at the interior of the edge occurs *via* a concerted displacement of a neighboring S atom. This leads to the simultaneous formation of an S_2 dimer and thiophene adsorbed on a double S-vacancy CUS. Their results suggest that these dynamic sulfur rearrangements are generally relevant to HDS reactions of a wider range of compounds. This explains why there is enough space for molecules such as dibenzothiophene to adsorb and undergo DDS on the edges of MoS_2. Thus, the adsorption-induced structural response at the MoS_2 edges demonstrates the dynamic nature of the catalyst under reaction conditions.

In this work, we investigated the effect of hydrogenation on the energetic stability, structural, and electronic properties of undoped and Ni- and Cu-doped MoS_2 S-edges under HDS reaction conditions using DFT calculations and an atomistic thermodynamic approach. We aim to understand how the formation of S–H bonds balances the energy cost associated with the rearrangement of the edge S atoms, and ultimately leads to the overall stabilization of the system. We also investigated the extent to which doping modifies the S–H bond strength, which is a key factor in the hydrogenation functionality of the catalyst.

2. Computational details

STM studies have demonstrated the favorable total substitution of Mo atoms at the S-edge with Fe, Co, Ni, and Cu atoms.[5,29] This has also been confirmed by previous DFT studies.[8,30] Therefore, our investigation focuses specifically on the S-edge, considering a complete replacement of the outermost Mo atoms with either Ni or Cu atoms. The slab supercell to model the doped S-edge is shown in Fig. 1. This slab exposes the dopant-substituted and fully S-saturated S-edge at the top, and the bare Mo-edge at the bottom before geometric optimization. Periodic boundary conditions were used, with 15 Å of vacuum in the *y*-direction and 9 Å of vacuum in the *z*-direction. The cell parameters used were 12.625, 26.845, and 12.068 Å. It is worth noting that the periodicity of the supercell in the *x*-direction could affect the stable S coverage, the formation of metal–metal dimers, and the S rearrangement. We choose a supercell size of four Mo in the *x*-direction to make a direct comparison with previous DFT studies on edge doping.[8,30,31]

Previous DFT studies have reported that the effect of transition metal substitution is to modify the binding strength of S at the edge, which is reflected in the S coverage.[8,31] A decrease in sulfur coverage is observed as the filling of the 3d band of the dopant metal increases. Several sulfur coverages were investigated, ranging from 12.5% to 100%, corresponding to 1 to 8 sulfur atoms at the edge. The sulfur coverages considered vary for the undoped S-edge from 50% to 100%, for the Ni-doped S-edge from 37.5% to 100%, and the Cu-doped edge from 12.5% to 100%. For the H species adsorbed on the edge, the adsorption of up to four H atoms was considered, corresponding to hydrogen coverages of 25%, 50%, 75%, and 100%. Our focus is only on the fully hydrogenated edges.

Spin-polarized DFT calculations were performed using the Vienna Ab Initio Simulation Package (VASP).[32,33] The Perdew–Burke–Ernzerhof exchange–correlation functional with a generalized gradient approximation was used.[34] The electron–ion

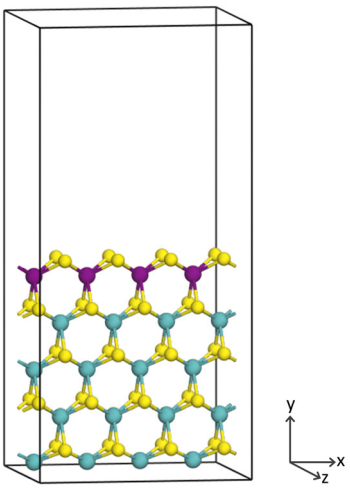

Fig. 1 Periodic model of the doped MoS_2 monolayer exposing the S-edge at the top. The turquoise, yellow, and purple spheres are the molybdenum, sulfur, and dopant atoms, respectively.

interactions were described employing the projector augmented wave (PAW) method,[35] and standard PAW potentials were used for all atoms with the following electron valence distributions: Mo $5s^1 4d^5$, Ni $4s^2 3d^8$, Cu $4s^1 3d^{10}$, S $3s^2 3p^4$, and H $1s^1$. A plane-wave kinetic energy cut-off of 400 eV was employed. To describe the partial occupancies of the electronic states, we used the Gaussian smearing method with a width of 0.05 eV and a convergence criterion of 10^{-5}. Similarly, the conjugate gradient algorithm was applied for ionic relaxation until convergence was reached with a criterion of 10^{-4} eV. All calculations include dipole corrections due to the nonsymmetric slab supercells.[8] A Monkhorst–Pack *k*-point mesh of $3 \times 1 \times 1$ was used for the slab calculations. All atoms were fully relaxed during the calculations. Bader charge[36] and electron density difference (EDD) analyses were performed to evaluate changes in the electronic structure. The EDD was calculated from the following equation:

$$\Delta\rho = \rho(\text{edge + adsorbate}) - \rho(\text{edge}) - \rho(\text{adsorbate}) \quad (1)$$

where ρ(edge + adsorbate) is the electron density of the whole system, ρ(edge) and ρ(adsorbate) are the electron densities of the edge, and the adsorbate is calculated at the adsorption positions, respectively. $\Delta\rho$ provides information about the electron density distribution upon adsorption, where positive values indicate a density gain and negative values indicate density loss. The VESTA program was used to visualize the electron density difference isosurfaces.[37]

The differential hydrogen adsorption energy (ΔE_H) for the final adsorbed H was calculated using the following equation:

$$\Delta E_H = E(\text{edge} + n\text{H}) - E(\text{edge} + (n-1)\text{H}) - \frac{1}{2}E(\text{H}_2) \quad (2)$$

where E(edge + nH) is the total energy for the S-edge structure with n adsorbed hydrogen atoms, E(edge + (n–1)H) is the total energy for (n–1) adsorbed hydrogen atoms and $E(H_2)$ is the energy of a gas phase hydrogen molecule.

2.1. Thermodynamic approach

To evaluate the stability of the S-edge at different sulfur coverages, we use the *ab initio* atomistic thermodynamics formalism proposed by Scheffler and Reuter.[38] This formulation assumes that the catalyst surface is in equilibrium with the gas phase and bulk reservoirs within the grand canonical ensemble. The stability of a given $M_zMo_xS_y$ edge composition can be determined by calculating the grand potential $\Omega(T,p)$, at temperature T and partial pressure p of the gas phase components. The thermodynamic formula for $\Omega(T,p)$ is

$$\Omega(T,p) = E^{\text{slab}}_{M_zMo_xS_y} - xE^{\text{bulk}}_{MoS_2} - \frac{z}{n}E^{\text{bulk}}_{M_nS_m} + \left(2x + \frac{m}{n}z - y\right)\mu_S(T,p) \quad (3)$$

where $E^{\text{slab}}_{M_zMo_xS_y}$ is the DFT total energy of the doped slab, containing x molybdenum atoms, y sulfur atoms, and z dopant atoms (M = Ni or Cu) and $E^{\text{bulk}}_{M_nS_m}$ is the DFT total energy of the dopant bulk phase (Ni_3S_2 and CuS) stable under the reaction conditions.[39] $\mu_S(T,p)$ is the chemical potential of sulfur, and it is determined by the chemical equilibrium with the gas phase mixture of H_2 and H_2S, giving

$$\mu_S(T,p) = \mu_{H_2S}(T,p) - \mu_{H_2}(T,p) = \left[\Delta E^{\text{mol}} + \Delta\tilde{\mu}_S(T,p^0) + RT\ln\left(\frac{p_{H_2S}}{p_{H_2}}\right)\right] \quad (4)$$

ΔE^{mol} is the difference between the DFT total energy of the H_2S and H_2 molecules $\left(E^{\text{mol}}_{H_2S} - E^{\text{mol}}_{H_2}\right)$, including zero-point vibrations. The term $\Delta\tilde{\mu}_S(T,p^0)$ corresponds to the difference between the thermal contributions to the chemical potential, which is calculated as $\left[\Delta\tilde{\mu}_S(T,p^0) = \tilde{\mu}_{H_2S}(T,p^0) - \tilde{\mu}_{H_2}(T,p^0)\right]$ and can be obtained from thermodynamic tables.[40] Here, p_{H_2S} and p_{H_2} denote the partial pressures of H_2S and H_2, respectively. The ratio $\frac{p_{H_2S}}{p_{H_2}}$ is used to indicate the relative abundance of H_2S and H_2 in the gas phase, with larger values indicating sulfur-rich conditions and smaller values indicating strongly reducing conditions where H_2 is more abundant than H_2S. Under HDS working conditions, the $\frac{p_{H_2S}}{p_{H_2}}$ ratio is typically between 0.01 and 0.05, while the temperature is in the range of 573 K to 700 K. For instance, representative HDS working conditions may include p_{H_2} = 10 bar, p_{H_2S} = 0.1 bar, and T = 650 K.[25]

For the hydrogenated edges, the grand potential can be expressed as

$$\Omega(T,p) = E^{\text{slab}}_{M_zMo_xS_yH_w} - xE^{\text{bulk}}_{MoS_2} - \frac{z}{n}E^{\text{bulk}}_{M_nS_m} + \left(2x + \frac{m}{n}z - y\right)\mu_S(T,p) - w\mu_H(T,p) \quad (5)$$

where

$$\mu_H(T,p) = \frac{1}{2}\mu_{H_2}(T,p) = \frac{1}{2}\left[E_{H_2} + \tilde{\mu}_{H_2}(T,p^0) + RT\ln\left(\frac{p_{H_2}}{p^0}\right)\right] \quad (6)$$

3. Results and discussion

3.1. Hydrogen adsorption on an undoped S-edge

To accurately describe hydrogen adsorption at the edge, the first step is to identify the stable edge configurations under the given reaction conditions. For a given sulfur coverage, several S adsorption configurations are possible. Fig. 2a–e show the most favorable edge configurations of the undoped S-edge for sulfur coverages between 50% and 100%. The edge configurations evaluated for each sulfur coverage are shown in Fig. S1 (ESI†). To evaluate the relative stability of the edge structures, we calculated the grand potential as a function of the p_{H_2S}/p_{H_2} partial pressure ratio at 650 K, as shown in Fig. 2f. At high p_{H_2S}/p_{H_2} ratios (sulfiding conditions), the most stable sulfur coverage is 100%, with the S atoms forming S_2 dimers every two bridging S atoms (100Mo_100S, Fig. 2e). Under typical HDS reaction conditions (T = 650 K, p_{H_2} = 10 bar, p_{H_2S}/p_{H_2} = 0.05–0.01), the most stable sulfur coverage is 50%, with the S atoms arranged in a zigzag configuration (100Mo_50S, Fig. 2a), as reported in previous DFT studies.[41,42]

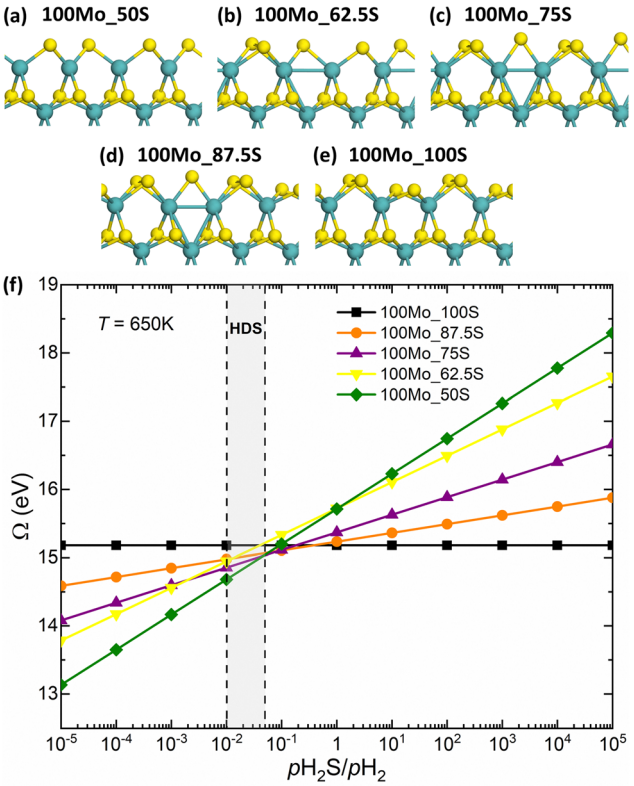

Fig. 2 (a)–(e) Optimized structures of the undoped S-edge for sulfur coverages between 50% and 100%. The turquoise and yellow spheres are the molybdenum and sulfur atoms, respectively. (f) Grand potential as a function of p_{H_2S}/p_{H_2} at 650 K.

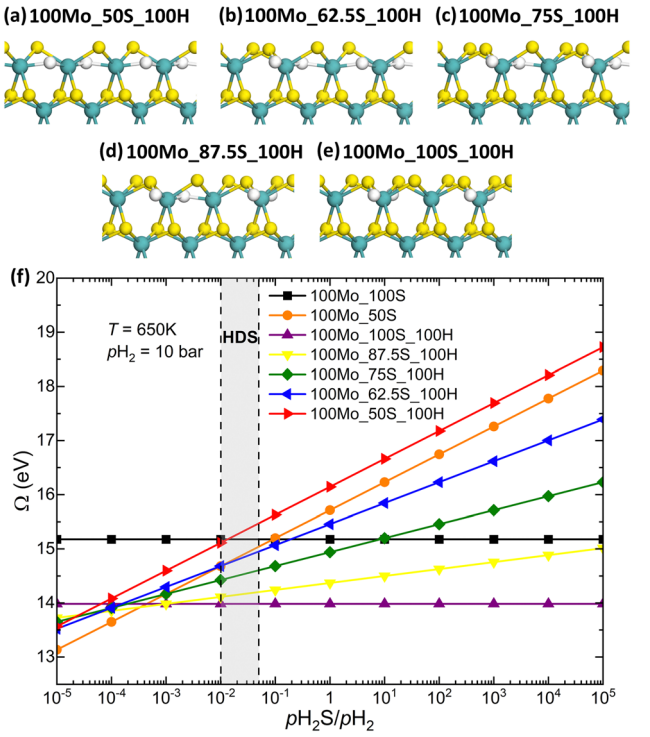

Fig. 3 (a)–(e) Optimized structures for different sulfur coverages of the undoped S-edge with 100% of hydrogen coverage. The turquoise, yellow, and white spheres are the molybdenum, sulfur, and hydrogen atoms, respectively. (f) Grand potential as a function of p_{H_2S}/p_{H_2} at 650 K and p_{H_2} = 10 bar.

As mentioned above, HDS operating conditions are sulfo-reductive conditions where H_2 is more abundant than H_2S in the gas phase. Hydrogen can interact with the edges of MoS_2 in two ways. First, the reaction of H_2 with the edge S atoms can reduce the sulfur coverage by forming H_2S. Second, the dissociative adsorption of H_2 can lead to the formation of SH or MoH groups. Therefore, we investigated the adsorption of hydrogen on the different structures in Fig. 2. For the undoped S-edge, the fully hydrogenated structures correspond to the dissociative adsorption of two H_2 molecules on the edge. The most favorable configurations of the hydrogenated S-edge for sulfur coverages between 50% and 100% are shown in Fig. 3. The edge configurations evaluated for H adsorption at each sulfur coverage are shown in Fig. S2 (ESI†). For the 50% sulfur coverage, the most favorable configuration corresponds to four bridging MoH groups (100Mo_50S_100H, Fig. 3a). This result is in agreement with that reported by Bruix *et al.*[43] for triangular MoS_2 nanoparticles exposing S-edges with 50% sulfur coverage. These authors suggested that MoS_2-based catalysts featuring edges with undercoordinated Mo atoms can accommodate H atoms in such bridging positions. This behavior is also observed for sulfur coverages between 62.5% and 87.5%. At 62.5% sulfur coverage, the adsorbed H atoms form three bridging MoH groups and one SH group (100Mo_62.5S_100H, Fig. 3b). At 75% sulfur coverage, they form two bridging MoH and two SH groups (100Mo_75S_100H, Fig. 3c). At 87.5% sulfur coverage, one bridging MoH and three SH groups are present (100Mo_87.5S_100H, Fig. 3d). At 100% sulfur coverage, the most favorable configuration corresponds to four alternating SH groups (100Mo_100S_100H, Fig. 3e). It is important to note that all of these edge structures have sulfur atoms arranged in a zigzag configuration without hydrogen adsorption (Fig. S2, ESI†). Thus, these structures can be seen as the result of the adsorption of H or SH groups on the 100Mo_50S structure.

Fig. 3f shows the grand potential as a function of the p_{H_2S}/p_{H_2} ratio at 650 K for the hydrogenated edge structures. The 100Mo_100S_100H structure shows the highest stability over a wide range of p_{H_2S}/p_{H_2} ratios. However, under strong reducing conditions, the 100Mo_50S structure is the most stable. Note that the 100Mo_50S structure is always more stable than the 100Mo_50S_100H structure, indicating that MoH or SH groups would not be present at low sulfur coverages, in agreement with Prodhomme *et al.*[25] Under HDS reaction conditions, the 100Mo_100S_100H structure is the most stable. The formation of the SH groups at 100% sulfur coverage has a strong stabilizing effect on the edge structure. It is worth noting that the hydrogenated structures 100Mo_62.5S_100H, 100Mo_75S_100H, and 100Mo_87.5S_100H are more stable than the 100Mo_50S structure and their stability increases as the sulfur coverage increases. Therefore, the mechanism of H_2 dissociation depends on the sulfur coverage of the edge where the dissociation occurs. Homolytic dissociation of H_2, leading exclusively to SH groups, is favored only at the fully sulfided S-edge, whereas the

heterolytic dissociation of H_2, forming MoH and SH groups, is favored at the partially sulfided edges.

Upon hydrogen adsorption, the S_2 dimers split, resulting in a shift of the S atoms. Therefore, we calculated the dissociative adsorption energy of H_2 and the energy cost associated with the rearrangement of S atoms for the 100Mo_100S_100H structure. The S atoms rearrangement energy ($\Delta E_{\text{Rearrag}}$) was calculated as the energy difference between the frozen edge in the geometry after hydrogen adsorption and the edge in its relaxed geometry before hydrogen adsorption. The dissociative adsorption energy of two H_2 molecules is exothermic by -2.27 eV (-1.14 eV/H_2) and the corresponding S rearrangement energy is 1.34 eV (0.67 eV/H_2) (Table 1). Thus, hydrogen adsorption involves a dynamic movement of the edge atoms in the process, which can be attributed to the large bending flexibility of the metal-sulfur bonds at the edges.[21]

The difference in the stability of the hydrogen species adsorbed at the edge may lie in the electronic properties, specifically in the reducibility of the Mo atoms involved. The stabilization of hydrogen as a proton species is formally an oxidation process and requires the reduction of Mo atoms, whereas the stabilization of hydrogen as a hydride species is a reduction process and involves the oxidation of Mo atoms.[44] Table 2 shows the Bader charges (q) of the edge atoms for the non-hydrogenated and hydrogenated structures with 50% and 100% sulfur coverage. The various adsorbed species at the edge with their respective formal charges are H^-, SH^-, S^{2-}, and S_2^{2-}. When H adsorbs to form SH groups in the 100Mo_50S structure, the excess electrons partially reduce the neighboring Mo atoms by about 0.17 e. Conversely, H adsorption as a hydride oxidizes the Mo atoms by about 0.12 e. Each H atom carries a negative charge of -0.31 e. For the S-dimer 100Mo_100S structure, the charge on the S atoms is found to be more negative as S^{2-} anions (-0.57 e) than as S_2^{2-} dimers (-0.26 e), consistent with the fact that the S atoms in the dimers are low-valence sulfur species, S^-.[45] Thus, by comparing the S-dimer and the S-bridge 100Mo_100S structures, it is observed that the replacement of the S_2^{2-} dimers by two S^{2-} anions has an oxidizing effect on the neighboring Mo atoms (each Mo atom loses about 0.08 e). For the 100Mo_100S_100H structure, it was found that the charge on the Mo atoms is almost the same as in the 100Mo_100S structure containing S_2^{2-} dimers (+1.25 e). This may be because the charge on the S atoms of the S_2^{2-} dimers is the same as that of the SH^- species (-0.26 e). Also, the charge of the S^{2-} anions is almost the same in both structures (-0.56 e). Therefore, the formation of SH groups in the S-dimer 100Mo_100S structure does not involve the reduction of Mo atoms. However, if the S-bridge 100Mo_100S structure is taken as a reference for the non-hydrogenated structure, the reduction of the Mo atoms is observed upon the formation of SH groups (each Mo atom gains 0.07 e). This process is also accompanied by the oxidation of the S atoms belonging to the SH groups. Recently, Khare *et al.*[44] pointed out that a higher electron density on Mo atoms should favor hydride formation, while a lower electron density on Mo atoms should favor sulfhydryl (SH) formation. This could explain the remarkable stability of the SH group formation on the 100Mo_100S structure compared to the 100Mo_50S structure. On the S-edge, Mo atoms with lower coordination tend to localize a higher electron density. Therefore, the formation of SH groups on the 100Mo_50S structure would reduce the Mo atoms to a less favorable oxidation state. However, the adsorption of H as hydride species on the 100Mo_50S structure is also less stable.

Table 1 The dissociative adsorption energy of H_2 and the corresponding S rearrangement energy for the most stable edge structures under reaction conditions

Edge configuration	ΔE_{ads} (H_2) (eV/H_2)	$\Delta E_{\text{Rearrag}}$ (eV/H_2)
100Mo_100S_100H	−1.14	0.67
100Ni_50S_100H	−0.78	0.93
100Cu_25S_50H	−1.84	0.18

As mentioned above, the hydrogenated structures 100Mo_50S_100H and 100Mo_100S_100H can be seen as a result of the adsorption of H or SH groups, respectively, onto the 100Mo_50S structure. To explain their different stability, it is necessary to understand the nature of the bonding between the H^- and SH^- species and the 100MoS_50S edge structure. We calculated the electron density difference to illustrate the redistribution of electron density due to the interaction between these species and the edge. In the EDD plots in Fig. 4, the blue regions represent electron density accumulation and the red regions represent electron density depletion. As shown in Fig. 4(a) and (b), the electron density accumulates between Mo–SH bonds but depletes between Mo–H bonds, suggesting a stronger interaction between SH^- species and Mo atoms. This may explain why stabilizing hydrogen as sulfhydryl groups at the S-edge is more thermodynamically favorable than stabilizing as hydrides.

3.2. Hydrogen adsorption on Ni-doped S-edge

To begin with the study of hydrogen adsorption on the Ni-doped S-edge, we first evaluated different configurations for S adsorption for sulfur coverages between 37.5% and 100%. Fig. 5a–f show the most favorable edge configurations. The edge configurations evaluated for each sulfur coverage are shown in Fig. S3 (ESI†). For sulfur coverages between 37.5% and 75%, Ni atoms tend to form Ni–Ni dimers as a result of the adsorption of S_2 dimers between them. This local edge reconstruction causes the Ni atoms to form a local structure with the S atoms that closely resembles a square planar environment, as previously reported in DFT studies.[8,30] Therefore, at low sulfur coverages, the S_2 dimers are located between two Ni–Ni dimers, while at high sulfur coverages, the S_2 dimers are located on top of the Ni atoms. This keeps the coordination number of the Ni atoms close to 4. Fig. 5g shows the grand potential as a function of the p_{H_2S}/p_{H_2} ratio at 650 K for the Ni-doped edge structures. It can be seen that under strong sulfiding conditions, the most stable sulfur coverage is 100% (100Ni_100S, Fig. 5f), while under strong reducing conditions the most stable sulfur coverage is 37.5% (100Ni_37.5S, Fig. 5a). Over a wide range of p_{H_2S}/

Table 2 Bader charges (q) for the non-hydrogenated and hydrogenated structures with 50% and 100% sulfur coverage for the undoped S-edge

Edge configuration	q_{Mo} (e)[a]	q_S (e)[b]	$q_{S(S_2)}$ (e)[c]	$q_{S(SH)}$ (e)[d]	q_H (e)[e]	$q_{H(SH)}$ (e)[f]
100Mo_50S $\begin{pmatrix} S \\ \square \end{pmatrix}\begin{pmatrix} \square \\ S \end{pmatrix}\begin{pmatrix} S \\ \square \end{pmatrix}\begin{pmatrix} \square \\ S \end{pmatrix}$	+1.15	−0.68	—	—	—	—
100Mo_50S_100H (S–H) $\begin{pmatrix} SH \\ \square \end{pmatrix}\begin{pmatrix} \square \\ SH \end{pmatrix}\begin{pmatrix} SH \\ \square \end{pmatrix}\begin{pmatrix} \square \\ SH \end{pmatrix}$	+0.98	—	—	−0.47	—	+0.02
100Mo_50S_100H (Mo–H) $\begin{pmatrix} S \\ H \end{pmatrix}\begin{pmatrix} H \\ S \end{pmatrix}\begin{pmatrix} S \\ H \end{pmatrix}\begin{pmatrix} H \\ S \end{pmatrix}$	+1.27	−0.59	—	—	−0.31	—
100Mo_100S (S-dimer) $(S_2)\begin{pmatrix} S \\ S \end{pmatrix}(S_2)\begin{pmatrix} S \\ S \end{pmatrix}$	+1.24	−0.57	−0.26	—	—	—
100Mo_100S (S-bridge) $\begin{pmatrix} S \\ S \end{pmatrix}\begin{pmatrix} S \\ S \end{pmatrix}\begin{pmatrix} S \\ S \end{pmatrix}\begin{pmatrix} S \\ S \end{pmatrix}$	+1.32	−0.48	—	—	—	—
100Mo_100S_100H $\begin{pmatrix} S \\ SH \end{pmatrix}\begin{pmatrix} SH \\ S \end{pmatrix}\begin{pmatrix} S \\ SH \end{pmatrix}\begin{pmatrix} SH \\ S \end{pmatrix}$	+1.25	−0.56	—	−0.29	—	+0.03

[a] q_{Mo} charge of the edge Mo atoms. [b] q_S charge of the single S atoms. [c] $q_{S(S_2)}$ charge of the S atom in the dimer. [d] $q_{S(SH)}$ charge of the S atom in the SH group. [e] q_H charge of the single H atoms. [f] $q_{H(SH)}$ charge of the H atom in the SH group.

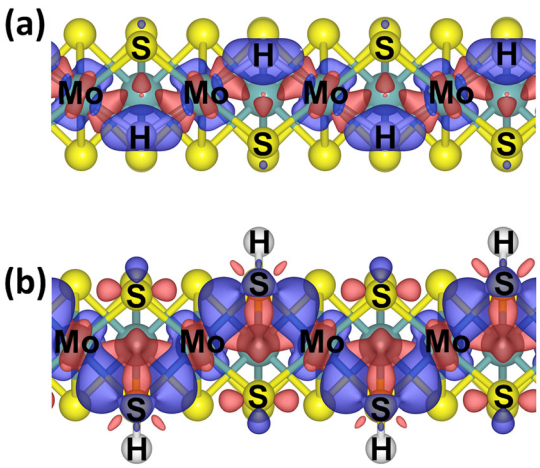

Fig. 4 Top view of the EDD plots for the (a) 100Mo_50S_100H and (b) 100Mo_100S_100H structures. The blue and red regions represent the electron density gain and loss, respectively. The EDD was plotted using an isodensity level of 0.0035 e bohr^{-3}.

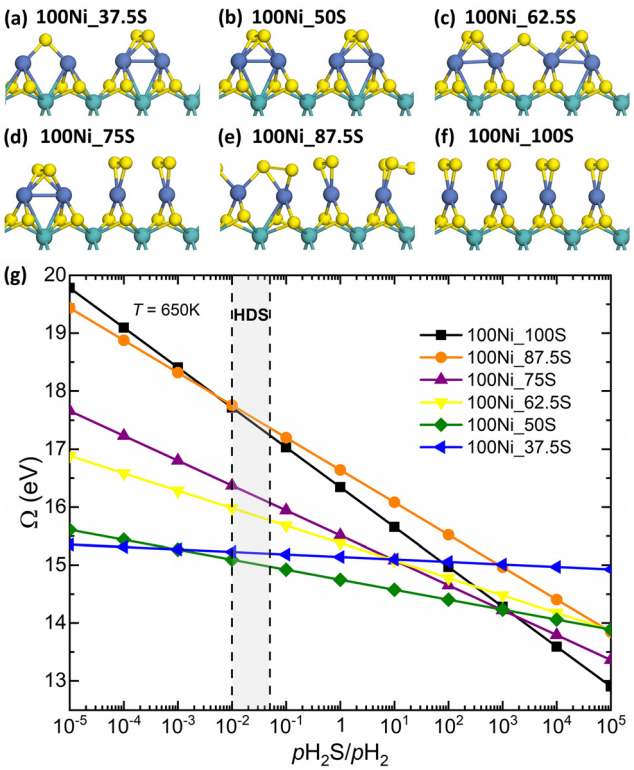

Fig. 5 (a)–(f) Optimized structures of the Ni-doped S-edge for sulfur coverages between 37.5% and 100%. The turquoise, blue, and yellow spheres are the molybdenum, nickel, and sulfur atoms, respectively. (g) Grand potential as a function of p_{H_2S}/p_{H_2} for the Ni-doped S-edge at 650 K.

p_{H_2} ratios, including HDS reaction conditions, the most stable sulfur coverage is 50% (100Ni_50S, Fig. 5b).

Experimental studies have shown that SH groups are the stable form of activated H on Ni-doped MoS_2.[46,47] To evaluate the formation of SH groups on the Ni-doped S-edge, we calculated the adsorption of hydrogen on the edge structure with 50% sulfur coverage, which is reported in Fig. 5 as the most stable under HDS reaction conditions. We also included the edge structure with 37.5% sulfur coverage to account for the formation of a sulfur vacancy at the edge. Fig. 6a–d show the two configurations evaluated for H adsorption for sulfur coverages of 37.5% and 50%. For instance, in the bridge-labeled configurations, the S atoms are adsorbed in a bridge position, while in the dimer-labeled configurations, the sulfur atoms are adsorbed as S_2 dimers between Ni–Ni dimers. Fig. 6d shows the grand potential as a function of the p_{H_2S}/p_{H_2} ratio at 650K for these hydrogenated edge structures. It can be seen that the 100Ni_50S_100H_bridge structure is the most stable in almost the entire range of p_{H_2S}/p_{H_2} ratios studied. It should be noted that the 100Ni_50S_100H_dimer structure is less stable than the 100Ni_50S structure, indicating that stable SH groups are not present in this configuration under reaction conditions. Therefore, the 100Ni_50S structure undergoes significant S rearrangement upon hydrogen adsorption. We found that the dissociative adsorption energy of two H_2 molecules to obtain the 100Ni_50S_100H_-bridge structure is exothermic to −1.55 eV (−0.78 eV/H_2), and the

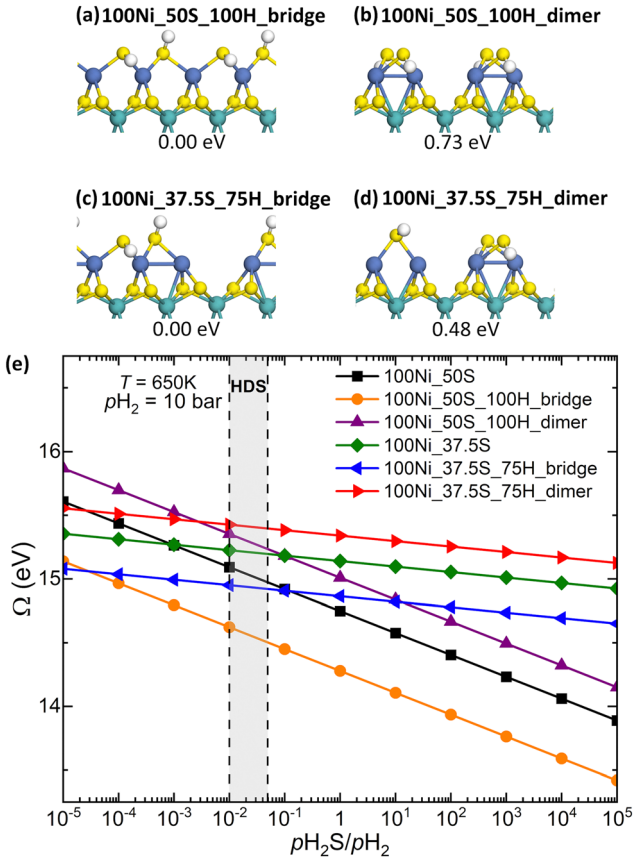

Fig. 6 Optimized structures for different configurations of the 100Ni_50S_100H structure, (a) 100Ni_50S_100H_bridge and (b) 100Ni_50S_100H_dimer, and the 100Ni_37.5S_75H structure, (c) 100Ni_37.5S_75H_bridge and (d) 100Ni_37.5S_75H_dimer. For a given sulfur coverage, the configurations of hydrogen adsorption are shown in order of decreasing stability. The turquoise, blue, yellow, and white spheres are the molybdenum, nickel, sulfur, and hydrogen atoms, respectively. Ε Grand potential as a function of p_{H_2S}/p_{H_2} at 650 K and p_{H_2} = 10 bar.

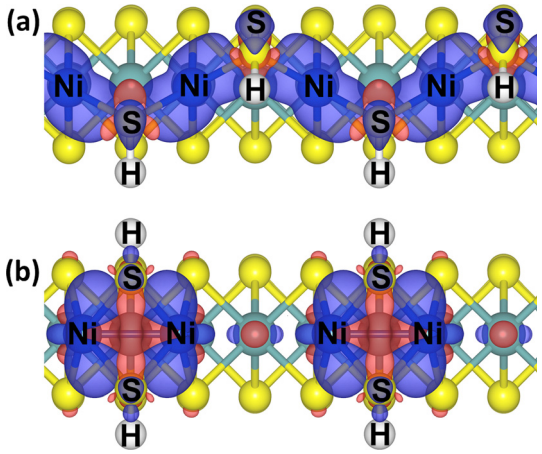

Fig. 7 Top view of the EDD plots for the (a) 100Ni_50S_100H_bridge and (b) 100Ni_50S_100H_dimer structures. The blue and red regions represent the electron density gain and loss, respectively. The EDD was plotted using an isodensity level of 0.003 e $borh^{-3}$.

energy cost associated with the S rearrangement is 1.85 eV (0.93 eV/H_2) (Table 1). Furthermore, by removing an S atom from the edge, the most stable hydrogenated structure is 100Ni_37.5S_75H_bridge. Note that this structure is more stable than the 100Ni_50S structure under reducing conditions, including HDS conditions, but its stability decreases when moving to sulfiding conditions. However, in the absence of hydrogen, the S-bridge configurations are less stable than the S-dimer configurations (Fig. S3, ESI†). Therefore, the formation of SH groups at the Ni-doped edge has a strong stabilizing effect despite the significant rearrangement of the S atoms. With this result, we could speculate that the dissociative adsorption of H_2 and the displacement of S atoms may occur with a concerted mechanism. However, a detailed kinetic analysis of such a concerted displacement is beyond the scope of the present work.

To gain insight into the underlying reason for the difference in stability between the 100Ni_50S_100H_dimer and 100Ni_50S_100H_bridge structures, Bader charge and electron density difference analyses were performed. Table 3 presents the Bader charges (q) of the edge atoms for the non-hydrogenated and hydrogenated structures of the dimer and bridge configurations with 50% sulfur coverage. When comparing the 100Ni_50S_dimer and 100Ni_50S_bridge structures, the oxidation of the Ni atoms is observed by replacing the S_2^{2-} dimers with two S_2^{2-} anions (each Ni atom loses about 0.07 e). This is also reflected in the calculated charges around the different sulfur species; the charge of the S^{2-} anions (−0.31 e) is more negative than around the S_2^{2-} dimers (−0.18 e). The formation of the SH groups has a weak oxidizing effect on the Ni atoms compared to the 100Ni_50S_dimer structure. For the 100Ni_50S_100H_dimer structure, the Ni atoms are oxidized by about 0.03 e upon hydrogen adsorption. In the 100Ni_50S_100H_bridge structure, each Ni atom loses about 0.04 e. However, the reduction of Ni atoms during the formation of SH groups is observed if the

Table 3 Bader charges (q) of the non-hydrogenated and hydrogenated structures with 50% sulfur coverage for the Ni-doped S-edge structures

Edge configuration	q_{Ni} (e)	q_{S} (e)	$q_{S(S_2)}$ (e)	$q_{S(SH)}$ (e)	$q_{H(SH)}$ (e)
100Ni_50S_dimer $(S_2)(\square)(S_2)(\square)$	+0.43	—	−0.18	—	—
100Ni_50S_bridge $\begin{pmatrix} S \\ \square \end{pmatrix}\begin{pmatrix} \square \\ S \end{pmatrix}\begin{pmatrix} S \\ \square \end{pmatrix}\begin{pmatrix} \square \\ S \end{pmatrix}$	+0.50	−0.31	—	—	—
100Ni_50S_100H_dimer $\begin{pmatrix} \square \\ \square \end{pmatrix}\begin{pmatrix} SH \\ SH \end{pmatrix}\begin{pmatrix} \square \\ \square \end{pmatrix}\begin{pmatrix} SH \\ SH \end{pmatrix}$	+0.46	—	—	−0.23	+0.03
100Ni_50S_100H_bridge $\begin{pmatrix} SH \\ \square \end{pmatrix}\begin{pmatrix} \square \\ SH \end{pmatrix}\begin{pmatrix} SH \\ \square \end{pmatrix}\begin{pmatrix} \square \\ SH \end{pmatrix}$	+0.47	—	—	−0.27	+0.02

100Ni_50S_bridge structure is taken as a reference for the non-hydrogenated structure. As in the undoped edge, this process also involves the oxidation of the S atoms belonging to the SH groups. Fig. 7a and b show the EDD plots for the 100Ni_50S_100H_bridge and 100Ni_50S_100H_dimer structures, respectively, using the densities of the SH groups as adsorbate references. In the 100Ni_50S_100H_bridge structure, there is a significant accumulation of electron density between the Ni–S bond, suggesting a strong interaction between the SH^- species and the Ni atoms.[48] In the 100Ni_50S_100H_dimer structure, a depletion region is observed close to the Ni atoms, which is not present in the 100Ni_50S_100H_bridge structure. Therefore, a large electron density redistribution occurs upon the rearrangement of S atoms. The movement of the S atoms during H adsorption may be driven by the electron density redistribution to reduce the repulsive interactions between the SH groups.

3.3. Hydrogen adsorption on Cu-doped S-edge

Fig. 8a–h show the most favorable configurations for the Cu-doped S-edge with sulfur coverages between 12.5% and 100%. The edge configurations evaluated for each sulfur coverage are shown in Fig. S4 (ESI†). At low sulfur coverages (12.5% and 37.5%), Cu atoms tend to form Cu–Cu dimers with only one S atom adsorbed between them. For sulfur coverages between 37.5% and 75%, the edge structures contain S_2 dimers. Each S atom of the dimer is bonded to a single Cu atom. This keeps the coordination number of Cu atoms close to 3, and the local structure that Cu atoms form with S atoms resembles a trigonal planar environment. At high sulfur coverages (87.5% and 100%), the edge structures are more complex. Here, each S atom of the dimer is bonded to an S atom from the edge. Fig. 8i shows the grand potential as a function of the p_{H_2S}/p_{H_2} ratio at 650 K for the Cu-doped edge structures. It can be seen that under strong sulfiding conditions, the most stable sulfur coverage is 50% (100Cu_50S, Fig. 8d). On the other hand, over a wide range of p_{H_2S}/p_{H_2} ratios, including reducing, HDS, and moderate sulfiding conditions, the most stable sulfur coverage is 25% (100Cu_25S, Fig. 8b). This result is consistent with the result reported by Tsai *et al.*[31] They found that group 11 metal dopants tend to have the lowest sulfur coverage, group 8 to 10 metal dopants have higher sulfur coverage, and group 5 to 7 metal dopants have the highest sulfur coverage.

To study the Cu-doped hydrogenated edge, we calculated the hydrogen adsorption on the edge structure with 25% sulfur coverage, which is shown in Fig. 8 as the most stable under HDS reaction conditions. We also included the edge structure with 12.5% sulfur coverage to account for the formation of a sulfur vacancy at the edge. For the Cu-doped S-edge, the fully hydrogenated edge results from the dissociative adsorption of one H_2 molecule at the edge. Fig. 9a and b show the side views for the optimized structures for H adsorption for sulfur coverages of 12.5% and 25%. Fig. 9c shows the grand potential as a function of the p_{H_2S}/p_{H_2} partial pressure ratio at 650 K. It can be seen that the 100Cu_25S_50H structure is the most stable over the whole range of p_{H_2S}/p_{H_2} ratios studied. On the other hand, the 100Cu_12.5S_25H structure is more stable than the

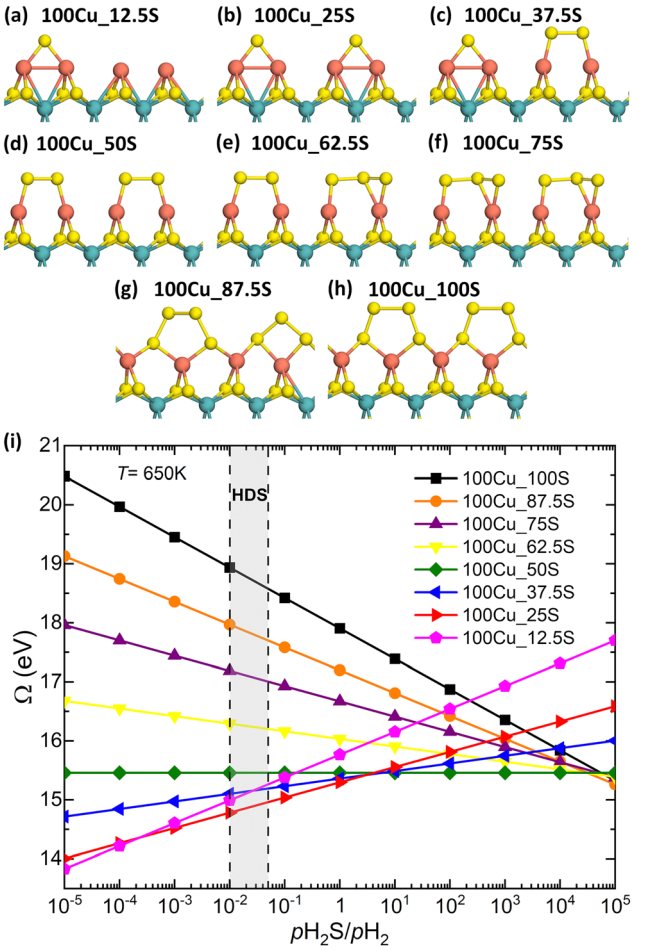

Fig. 8 (a)–(h) Optimized structures of the Cu-doped S-edge for sulfur coverages between 12.5% and 100%. The turquoise, orange, and yellow spheres are the molybdenum, copper, and sulfur atoms, respectively. (i) Grand potential as a function of p_{H_2S}/p_{H_2} for the Cu-doped S-edge at 650 K.

100Cu_25S structure over a wide range of p_{H_2S}/p_{H_2} ratios, including reducing, HDS, and moderate sulfiding conditions. Again, we found that the formation of SH groups has a strong stabilizing effect on the edge structure. We also found that the dissociative adsorption energy of an H_2 molecule is exothermic to −1.84 eV, and the S rearrangement energy is 0.18 eV (Table 1). Therefore, when H is adsorbed, the rearrangement of the S atoms is negligible. Table 4 shows the Bader charges (q) of the edge atoms for the non-hydrogenated and hydrogenated structures with 25% sulfur coverage. In the 100Cu_25S_50H structure, the formation of the SH groups has a weak reducing effect on the Cu atoms compared to the 100Cu_25S structure (each Cu atom gains 0.04 e). The oxidation of S atoms belonging to SH groups is also observed.

3.4. Insight into the hydrogenation properties of the doped S-edges

An important factor to examine is the adsorption strength of hydrogen on the doped edges. Kibsgaard *et al.*[5] pointed out that the variations in the binding of H could be an overriding factor

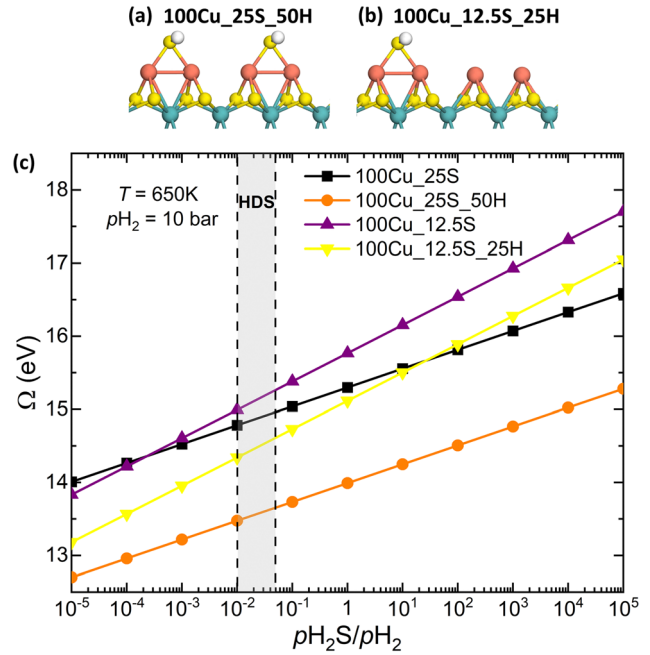

Fig. 9 Optimized structures for the (a) 100Cu_25S_50H and (b) 100Cu_12.5S_25H edge structures. The turquoise, orange, yellow, and white spheres are the molybdenum, copper, sulfur, and hydrogen atoms, respectively. (c) Grand potential as a function of p_{H_2S}/p_{H_2} at 650 K and p_{H_2} = 10 bar.

Table 4 Bader charges (q) of the non-hydrogenated and hydrogenated structures with 25% sulfur coverage for the Cu-doped S-edge

Edge configuration	q_{Cu} (e)	q_S (e)	$q_{S(SH)}$ (e)	$q_{H(SH)}$ (e)
100Cu_25S (S)(□)(S)(□)	+0.48	−0.51	—	—
100Cu_25S_50H (SH)(□)(SH)(□)	+0.44	—	−0.36	+0.01

determining both the DDS and HYD pathways, since a too weak/strong binding of H would significantly impede the key reaction steps involving the transfer of H from the edges. On the other hand, SH groups are known to exhibit Brønsted acidic character.[49,50] The strength of Brønsted acidity is related to the strength of H adsorption. Therefore, a weaker S–H bond results in a hydrogen atom that is more acidic and more easily deprotonated.[51–54] Table 5 shows the calculated differential hydrogen adsorption energy (ΔE_H), for the final adsorbed H on the 100Ni_50S_100H_bridge, 100Mo_100S_100H and 100Cu_25S_50H structures. It was found that the hydrogen adsorption strength at the S-edge shows the following trend:

Table 5 The differential hydrogen adsorption energy (ΔE_H) for the final adsorbed hydrogen and the Bader charge on the S atoms of the SH group for the undoped and doped S-edge

Edge configuration	ΔE_H (eV)	$q_{S(SH)}$ (e)
100Ni_50S_100H_bridge	−0.48	−0.27
100Mo_100S_100H	−0.60	−0.29
100Cu_25S_50H	−0.90	−0.36

Cu-doped > undoped > Ni-doped. This trend is opposite to that observed for hydrogenation catalytic activity,[5,8] suggesting that lower activity may be associated with stronger H bonding. The hydrogen atom on the 100Ni_50S_100H_bridge structure has the lowest ΔE_H. This would be the most Brønsted acidic hydrogen and the most likely to be removed from the edge. In contrast, the hydrogen atom on the 100Cu_25S_50H structure is the most strongly bound to the edge and therefore should be the least acidic and the most difficult to remove. We also calculated the Bader charge of the S atoms belonging to the SH group. The negative charge on the S atom decreases in the following order: Cu-doped > undoped > Ni-doped. Within these results, we speculate that the Ni doping could decrease the basicity of the S atoms compared to the undoped S-edge, leading to an increase in the Brønsted acidity of the S–H groups. Consequently, this would enhance the proton transfer ability in the SH groups, which is a key for an active hydrogenation catalyst. In contrast, the Cu doping could lead to a poisoning effect by increasing the basicity of the S atoms. This results in strongly adsorbed H, which cannot act as a reactive H species. It is important to note that the Brønsted acid nature of the SH groups should be confirmed by the adsorption of basic molecules such as ammonia, pyridine, and lutidine.[51,54–57] However, this is outside the scope of the present study.

4. Conclusions

In this work, we have carried out a comprehensive theoretical analysis of S atom rearrangement on the Ni and Cu-doped MoS_2 S-edge upon hydrogen adsorption under HDS reaction conditions. Our results show that SH groups are the stable form of hydrogen adsorption and have a strong stabilization effect on the edges. For the undoped S-edge, the most stable structure corresponds to 100% coverage of sulfur and hydrogen. This structure shows a shift of the S atoms caused by the splitting of the S_2 dimers. For the Ni-doped S-edge, the most stable structure is one with 50% sulfur and 100% hydrogen coverage. This particular structure results from a significant rearrangement of the edge S atoms upon hydrogen adsorption. For the Cu-doped S-edge, the most stable structure is achieved with 25% sulfur and 50% hydrogen coverage. This structure shows minimal rearrangement of the S atoms. Therefore, the dynamic nature of the S atoms is demonstrated by the structural response of the edges to H adsorption. This suggests that the edge equilibrium structure can be significantly perturbed by the reaction conditions.

Using hydrogen adsorption strength as a simple probe of hydrogenation activity, our results suggest that the promoting effect of Ni may be associated with decreased S–H bond strength, whereas the poisoning effect of Cu may be associated with increased S–H bond strength. For the HDS reaction, it is essential that the hydrogen adsorption is exothermic to ensure that reactive hydrogen species are available at the edge. However, the hydrogen adsorption should not be too exothermic as this would reduce the availability of these hydrogen species for the hydrogenation steps.

Conflicts of interest

There are no conflicts to declare.

References

1 H. Topsøe, B. S. Clausen and F. E. Massoth, *Catalysis*, Springer Berlin Heidelberg, Berlin, Heidelberg, 1996, p. 459.
2 *Catalysis by Transition Metal Sulphides: From Molecular Theory to Industrial Application*, ed. H. Toulhoat and P. Raybaud, Editions Technip, Paris, 2013.
3 X. Li, A. Wang, M. Egorova and R. Prins, Kinetics of the HDS of 4,6-dimethyldibenzothiophene and its hydrogenated intermediates over sulfided Mo and NiMo on γ-Al_2O_3, *J. Catal.*, 2007, **250**, 283–293.
4 E. Krebs, B. Silvi, A. Daudin and P. Raybaud, A DFT study of the origin of the HDS/HydO selectivity on Co(Ni)MoS active phases, *J. Catal.*, 2008, **260**, 276–287.
5 J. Kibsgaard, A. Tuxen, K. G. Knudsen, M. Brorson, H. Topsøe, E. Lægsgaard, J. V. Lauritsen and F. Besenbacher, Comparative atomic-scale analysis of promotional effects by late 3d-transition metals in MoS_2 hydrotreating catalysts, *J. Catal.*, 2010, **272**, 195–203.
6 H. Topsøe, B. S. Clausen, R. Candia, C. Wivel and S. Mørup, In situ Mössbauer emission spectroscopy studies of unsupported and supported sulfided CoMo hydrodesulfurization catalysts: Evidence for and nature of a CoMoS phase, *J. Catal.*, 1981, **68**, 433–452.
7 N. Y. Topsøe and H. Topsøe, Characterization of the structures and active sites in sulfided CoMo/Al_2O_3 and NiMo/Al_2O_3 catalysts by NO chemisorption, *J. Catal.*, 1983, **84**, 386–401.
8 R. Arancon, M. Saab, A. Morvan, A. Bonduelle-Skrzypczak, A.-L. Taleb, A.-S. Gay, C. Legens, O. Ersen, K. Searles, V. Mougel, A. Fedorov, C. Copéret and P. Raybaud, Combined Experimental and Theoretical Molecular Approach of the Catalytically Active Hydrotreating MoS_2 Phases Promoted by 3d Transition Metals, *J. Phys. Chem. C*, 2019, **123**, 24659–24669.
9 P. Raybaud, J. Hafner, G. Kresse, S. Kasztelan and H. Toulhoat, Ab Initio Study of the H_2–H_2S/MoS_2 Gas–Solid Interface: The Nature of the Catalytically Active Sites, *J. Catal.*, 2000, **189**, 129–146.
10 N. Y. Topsøe, H. Topsøe and F. E. Massoth, Evidence of Brønsted acidity on sulfided promoted and unpromoted Mo/Al_2O_3 catalysts, *J. Catal.*, 1989, **119**, 252–255.
11 N. Salazar, S. B. Schmidt and J. V. Lauritsen, Adsorption of nitrogenous inhibitor molecules on MoS_2 and CoMoS hydrodesulfurization catalysts particles investigated by scanning tunneling microscopy, *J. Catal.*, 2019, **370**, 232–240.
12 M. V. Bollinger, K. W. Jacobsen and J. K. Nørskov, Atomic and electronic structure of MoS_2 nanoparticles, *Phys. Rev. B: Condens. Matter Mater. Phys.*, 2003, **67**, 085410.
13 J. V. Lauritsen, M. V. Bollinger, E. Lægsgaard, K. W. Jacobsen, J. K. Nørskov, B. S. Clausen, H. Topsøe and F. Besenbacher, Atomic-scale insight into structure and morphology changes of MoS_2 nanoclusters in hydrotreating catalysts, *J. Catal.*, 2004, **221**, 510–522.
14 F. Bataille, J.-L. Lemberton, P. Michaud, G. Pérot, M. Vrinat, M. Lemaire, E. Schulz, M. Breysse and S. Kasztelan, Alkyldibenzothiophenes Hydrodesulfurization-Promoter Effect, Reactivity, and Reaction Mechanism, *J. Catal.*, 2000, **191**, 409–422.
15 M. Egorova and R. Prins, Hydrodesulfurization of dibenzothiophene and 4,6-dimethyldibenzothiophene over sulfided NiMo/γ-Al_2O_3, CoMo/γ-Al_2O_3, and Mo/γ-Al_2O_3 catalysts, *J. Catal.*, 2004, **225**, 417–427.
16 J. V. Lauritsen, M. Nyberg, J. K. Nørskov, B. S. Clausen, H. Topsøe, E. Lægsgaard and F. Besenbacher, Hydrodesulfurization reaction pathways on MoS_2 nanoclusters revealed by scanning tunneling microscopy, *J. Catal.*, 2004, **224**, 94–106.
17 E. M. Morales-Valencia, C. O. Castillo-Araiza, S. A. Giraldo and V. G. Baldovino-Medrano, Kinetic Assessment of the Simultaneous Hydrodesulfurization of Dibenzothiophene and the Hydrogenation of Diverse Polyaromatic Structures, *ACS Catal.*, 2018, **8**, 3926–3942.
18 A. S. Walton, J. V. Lauritsen, H. Topsøe and F. Besenbacher, MoS_2 nanoparticle morphologies in hydrodesulfurization catalysis studied by scanning tunneling microscopy, *J. Catal.*, 2013, **308**, 306–318.
19 N. Y. Topsoe and H. Topsoe, FTIR Studies of Mo/Al_2O_2-Based Catalysts, *J. Catal.*, 1993, **139**, 641–651.
20 S. S. Grønborg, N. Salazar, A. Bruix, J. Rodríguez-Fernández, S. D. Thomsen, B. Hammer and J. V. Lauritsen, Visualizing hydrogen-induced reshaping and edge activation in MoS_2 and Co-promoted MoS_2 catalyst clusters, *Nat. Commun.*, 2018, **9**, 2211.
21 L. S. Byskov, M. Bollinger, J. K. Nørskov, B. S. Clausen and H. Topsøe, Molecular aspects of the H_2 activation on MoS_2 based catalysts—the role of dynamic surface arrangements, *J. Mol. Catal. A: Chem.*, 2000, **163**, 117–122.
22 S. Cristol, J. F. Paul, E. Payen, D. Bougeard, S. Clémendot and F. Hutschka, Theoretical Study of the MoS_2 (100) Surface: A Chemical Potential Analysis of Sulfur and Hydrogen Coverage. 2. Effect of the Total Pressure on Surface Stability, *J. Phys. Chem. B*, 2002, **106**, 5659–5667.
23 A. Travert, H. Nakamura, R. A. van Santen, S. Cristol, J.-F. Paul and E. Payen, Hydrogen Activation on Mo-Based Sulfide Catalysts, a Periodic DFT Study, *J. Am. Chem. Soc.*, 2002, **124**, 7084–7095.
24 M. Sun, A. Nelson and J. Adjaye, *Ab initio* DFT study of hydrogen dissociation on MoS_2, NiMoS, and CoMoS: mechanism, kinetics, and vibrational frequencies, *J. Catal.*, 2005, **233**, 411–421.
25 P.-Y. Prodhomme, P. Raybaud and H. Toulhoat, Free-energy profiles along reduction pathways of MoS_2 M-edge and S-edge by dihydrogen: A first-principles study, *J. Catal.*, 2011, **280**, 178–195.
26 R. Kronberg, M. Hakala, N. Holmberg and K. Laasonen, Hydrogen adsorption on MoS_2-surfaces: a DFT study on preferential sites and the effect of sulfur and hydrogen coverage, *Phys. Chem. Chem. Phys.*, 2017, **19**, 16231–16241.

27 C. Tsai, K. Chan, J. K. Nørskov and F. Abild-Pedersen, Understanding the Reactivity of Layered Transition-Metal Sulfides: A Single Electronic Descriptor for Structure and Adsorption, *J. Phys. Chem. Lett.*, 2014, **5**, 3884–3889.
28 N. Salazar, S. Rangarajan, J. Rodríguez-Fernández, M. Mavrikakis and J. V. Lauritsen, Site-dependent reactivity of MoS_2 nanoparticles in hydrodesulfurization of thiophene, *Nat. Commun.*, 2020, **11**, 4369.
29 J. Lauritsen, J. Kibsgaard, G. Olesen, P. Moses, B. Hinnemann, S. Helveg, J. Nørskov, B. Clausen, H. Topsoe and E. Lagsgaard, Location and coordination of promoter atoms in Co- and Ni-promoted MoS_2-based hydrotreating catalysts, *J. Catal.*, 2007, **249**, 220–233.
30 E. Krebs, B. Silvi and P. Raybaud, Mixed sites and promoter segregation: A DFT study of the manifestation of Le Chatelier's principle for the Co(Ni)MoS active phase in reaction conditions, *Catal. Today*, 2008, **130**, 160–169.
31 C. Tsai, K. Chan, J. K. Nørskov and F. Abild-Pedersen, Rational design of MoS_2 catalysts: tuning the structure and activity via transition metal doping, *Catal. Sci. Technol.*, 2015, **5**, 246–253.
32 G. Kresse and J. Hafner, *Ab initio* molecular dynamics for liquid metals, *Phys. Rev. B: Condens. Matter Mater. Phys.*, 1993, **47**, 558–561.
33 G. Kresse and J. Furthmüller, Efficient iterative schemes for *ab initio* total-energy calculations using a plane-wave basis set, *Phys. Rev. B: Condens. Matter Mater. Phys.*, 1996, **54**, 11169–11186.
34 J. P. Perdew, K. Burke and M. Ernzerhof, Generalized Gradient Approximation Made Simple, *Phys. Rev. Lett.*, 1996, **77**, 3865–3868.
35 G. Kresse and D. Joubert, From ultrasoft pseudopotentials to the projector augmented-wave method, *Phys. Rev. B: Condens. Matter Mater. Phys.*, 1999, **59**, 1758–1775.
36 R. F. W. Bader, A quantum theory of molecular structure and its applications, *Chem. Rev.*, 1991, **91**, 893–928.
37 K. Momma and F. Izumi, *VESTA 3* for three-dimensional visualization of crystal, volumetric and morphology data, *J. Appl. Crystallogr.*, 2011, **44**, 1272–1276.
38 K. Reuter and M. Scheffler, Composition, structure, and stability of RuO_2 (110) as a function of oxygen pressure, *Phys. Rev. B: Condens. Matter Mater. Phys.*, 2001, **65**, 035406.
39 R. R. Chianelli, T. A. Pecoraro, T. R. Halbert, W. H. Pan and E. I. Stiefel, Transition metal sulfide catalysis: Relation of the synergic systems to the periodic trends in hydrodesulfurization, *J. Catal.*, 1984, **86**, 226–230.
40 M. W. Chase Jr., NIST-JANAF Thermochemical Tables, *J. Phys. Chem. Ref. Data, Monogr.*, 1998, **9**, 1–1951.
41 H. Schweiger, P. Raybaud, G. Kresse and H. Toulhoat, Shape and Edge Sites Modifications of MoS_2 Catalytic Nanoparticles Induced by Working Conditions: A Theoretical Study, *J. Catal.*, 2002, **207**, 76–87.
42 A. Nelson, M. Sun and A. Junaid, On the structure and composition of the phosphosulfide overlayer on Ni_2P at hydrotreating conditions, *J. Catal.*, 2006, **241**, 180–188.
43 A. Bruix, J. V. Lauritsen and B. Hammer, Effects of particle size and edge structure on the electronic structure, spectroscopic features, and chemical properties of Au(111)-supported MoS_2 nanoparticles, *Faraday Discuss.*, 2016, **188**, 323–343.
44 R. Khare, R. Weindl, A. Jentys, K. Reuter, H. Shi and J. A. Lercher, Di- and Tetrameric Molybdenum Sulfide Clusters Activate and Stabilize Dihydrogen as Hydrides, *JACS Au*, 2022, **2**, 613–622.
45 J. Duchet, E. van Oers, V. de Beer and R. Prins, Carbon-supported sulfide catalysts, *J. Catal.*, 1983, **80**, 386–402.
46 E. Schachtl, J. S. Yoo, O. Y. Gutiérrez, F. Studt and J. A. Lercher, Impact of Ni promotion on the hydrogenation pathways of phenanthrene on MoS_2/γ-Al_2O_3, *J. Catal.*, 2017, **352**, 171–181.
47 W. Luo, H. Shi, E. Schachtl, O. Y. Gutiérrez and J. A. Lercher, Active Sites on Nickel-Promoted Transition-Metal Sulfides That Catalyze Hydrogenation of Aromatic Compounds, *Angew. Chem., Int. Ed.*, 2018, **57**, 14555–14559.
48 X. Hong, K. Chan, C. Tsai and J. K. Nørskov, How Doped MoS_2 Breaks Transition-Metal Scaling Relations for CO_2 Electrochemical Reduction, *ACS Catal.*, 2016, **6**, 4428–4437.
49 N. Y. Topsoe and H. Topsoe, FTIR Studies of Mo/Al_2O_3-Based Catalysts, *J. Catal.*, 1993, **139**, 641–651.
50 G. Berhault, M. Lacroix, M. Breysse, F. Maugé, J.-C. Lavalley, H. Nie and L. Qu, Characterization of Acidic Sites of Silica-Supported Transition Metal Sulfides by Pyridine and 2,6 Dimethylpyridine Adsorption: Relation to Activity in CH_3SH Condensation, *J. Catal.*, 1998, **178**, 555–565.
51 Á. Logadóttir, P. G. Moses, B. Hinnemann, N.-Y. Topsøe, K. G. Knudsen, H. Topsøe and J. K. Nørskov, A density functional study of inhibition of the HDS hydrogenation pathway by pyridine, benzene, and H_2S on MoS_2-based catalysts, *Catal. Today*, 2006, **111**, 44–51.
52 S. Rangarajan and M. Mavrikakis, DFT Insights into the Competitive Adsorption of Sulfur- and Nitrogen-Containing Compounds and Hydrocarbons on Co-Promoted Molybdenum Sulfide Catalysts, *ACS Catal.*, 2016, **6**, 2904–2917.
53 H. Cai, R. Schimmenti, H. Nie, M. Mavrikakis and Y.-H. C. Chin, Mechanistic Role of the Proton–Hydride Pair in Heteroarene Catalytic Hydrogenation, *ACS Catal.*, 2019, **9**, 9418–9437.
54 D. Lin and S. Rangarajan, A DFT study of site-dependent energetics of hexagonal MoS_2 nanoparticles under varying reaction conditions, *Surf. Sci.*, 2023, **729**, 122231.
55 B. Temel, A. K. Tuxen, J. Kibsgaard, N.-Y. Topsøe, B. Hinnemann, K. G. Knudsen, H. Topsøe, J. V. Lauritsen and F. Besenbacher, Atomic-scale insight into the origin of pyridine inhibition of MoS_2-based hydrotreating catalysts, *J. Catal.*, 2010, **271**, 280–289.
56 S. S. Grønborg, N. Salazar, A. Bruix, J. Rodríguez-Fernández, S. D. Thomsen, B. Hammer and J. V. Lauritsen, Visualizing hydrogen-induced reshaping and edge activation in MoS_2 and Co-promoted MoS_2 catalyst clusters, *Nat. Commun.*, 2018, **9**, 2211.
57 N. Salazar, S. B. Schmidt and J. V. Lauritsen, Adsorption of nitrogenous inhibitor molecules on MoS_2 and CoMoS hydrodesulfurization catalysts particles investigated by scanning tunneling microscopy, *J. Catal.*, 2019, **370**, 232–240.

